Experimentally distinguishing electro-optic effects in silicon

Jingcheng Zhu (朱景程)[1], Zhanguo Chen (陈占国)[1*], Xiuhuan Liu (刘秀环)[2], Jinbo Mu (牟晋博)[1], Yanjun Gao (高延军)[1], Wei Han (韩 伟)[3], and Gang Jia (贾 刚)[1]

[1]*State Key Laboratory on Integrated Optoelectronics, College of Electronic Science and Engineering, Jilin University, Changchun 130012, China*

[2]*College of Communication Engineering, Jilin University, Changchun 130012, China*

[3]*Changchun Telecom Engineering Designing Institute, Jilin University, Changchun 130012, China*

[*]*Corresponding author: czg@jlu.edu.cn*

Received February 13, 2012; accepted March 26, 2012; posted online June 15, 2012

Different electro-optic effects, such as Kerr effect, Pockels effect induced by the electric field or strain, and plasma dispersion effect exist in silicon. Experimentally distinguishing these effects is necessary for designing silicon-based electro-optic devices. According to their different polarization dependencies and frequency responses, these effects are measured and distinguished successfully via a transverse electro-optic modulation experiment based on the near-intrinsic silicon sample. The results indicate that Pockels effect induced by the electric field or strain is primary among these effects in the near-intrinsic silicon sample.

OCIS codes: 230.2090, 190.3270, 260.1440.
doi: 10.3788/COL201210.082301.

Silicon is an important semiconductor, not only as the microelectronic material, but also for electro-optic applications[1−3]. In recent years, silicon optical modulators[4−6] have been widely investigated because they are the key components of integrated optical circuits. Silicon optical modulators are mainly based on thermo-optic[7,8] and electro-optic[9] effects. Electro-optic effects have faster response than thermo-optic effects; thus, they are the more promising mechanisms of silicon optical modulators. The electro-optic effects in silicon can be classified into two types: 1) direct electro-optic effects such as Kerr effect (KE)[10] and Pockels effect (PE)[11], by which the applied electric field can change the real part of the refractive index directly, and 2) indirect electro-optic effects such as Franz-Keldysh effect (FKE)[12] and plasma dispersion effect (PDE)[13], by which the applied electric field is able to alter the absorption coefficient or the imaginary part of the refractive index, thereby also indirectly changing the real part of the refractive index according to the Kramers-Kronig relations. PDE is generally much stronger than other electro-optic effects in doped silicon. Therefore, it has become the main operating mechanism of most silicon optical modulators. In fact, in addition to PDE, other electro-optic effects exist in silicon optical modulators. In some situations (e.g., in intrinsic or near-intrinsic silicon crystals), because carrier density is low, other electro-optic effects cannot be negligible, and become even stronger than PDE. Therefore, distinguishing these electro-optic effects in silicon is necessary and significant. Soref *et al.*[9] theoretically calculated and compared these electro-optic effects in silicon; however, they did not experimentally detect and distinguish them.

In this letter, an electro-optic modulation experiment of near-intrinsic silicon is conducted to draw a distinction among these effects according to their different polarization dependencies and frequency properties.

Both PE and KE can directly change the refractive index of a material in response to an applied electric field. KE exists in all materials. KE is also called the quadratic electro-optic effect because the induced change of the refractive index is quadratic in the electric field E (i.e., $\Delta n \propto E^2$). In contrast, PE occurs only in crystals without inversion symmetry. PE is also called the linear electro-optic effect because the induced change of the refractive index is proportional to the electric field (i.e., $\Delta n \propto E$). Silicon belongs to the m3m point group; therefore, an ideal silicon crystal has inverse symmetry. Thus, PE is absent in bulk and unstrained silicon according to the dipole approximation. However, near the surfaces and interfaces or in the space charge regions of silicon, the inversion symmetry of silicon can be broken naturally or by built-in electric field[14,15] and strain[16,17]. Therefore, the electric-field-induced[11,18] or strain-induced[19,20] PE can also take place in silicon. Both PE and KE are able to produce the birefringence in silicon.

Provided that a sine wave signal $E = E_{\rm m}\cos(\Omega t)$ is applied on the (111)-cut silicon sample along the direction of [111], silicon will become a uniaxial crystal with the optical axis [111] according to the theory of KE. The difference between the refractive indices of the extraordinary ray and the ordinary ray can be obtained by

$$\Delta n_{\rm KE} = s_{44} n_{\rm b0}^3 E_{\rm m}^2 [\cos(2\Omega t) + 1]/2, \qquad (1)$$

where s_{44} is the Kerr coefficient of silicon and $n_{\rm b0}$ is the refractive index of the bulk silicon without the electric field.

KE is the bulk effect of silicon. In addition to KE, PE should also be taken into account at the surfaces or interfaces of silicon. As for (111)-Si crystals, 3 m symmetry has been verified at the surfaces of silicon[11,19], and the optical axis is the [111] axis. Therefore, under the electric field $E = E_{\rm m}\cos(\Omega t)$ along the [111] direction, silicon surfaces remain uniaxial, and the orientations of the principal axes are unchanged. The birefringence of

silicon surfaces can be deduced as

$$\Delta n_{\rm PE} = (n_{\rm se} - n_{\rm so}) - (\gamma_{33} n_{\rm se}^3 - \gamma_{13} n_{\rm so}^3) E_{\rm m} \cos(\Omega t)/2, \quad (2)$$

where $n_{\rm se} \approx n_{\rm so}$ are indices of the extraordinary ray and the ordinary ray at silicon surfaces, and γ_{13} and γ_{33} are effective Pockels coefficients directly relevant to the effective second-order susceptibility $\chi^{(2)}_{\mu\alpha\beta,\rm eff}(\mu,\alpha,\beta{=}1,2,3)$ of silicon (i.e.,$\gamma_{\mu l} = 2\chi^{(2)}_{\mu\alpha\beta,\rm eff}/\varepsilon_{\mu\mu}\varepsilon_{\alpha\alpha}(l = 1,2,\cdots,6)$ according to the nonlinear optics). Here, $\chi^{(2)}_{\rm eff}$ may include the contributions from surfaces, the built-in field, and the strain (i.e., $\chi^{(2)}_{\rm eff} \sim \chi^{(2)}_{\rm S} + \chi^{(2)}_{\rm EI} + \chi^{(2)}_{\rm SI}$); $\chi^{(2)}_{\rm S}$ is the surface second-order susceptibility; $\chi^{(2)}_{\rm EI}$ and $\chi^{(2)}_{\rm SI}$ are the electric-field-induced and the strain-induced second-order susceptibilities of silicon, respectively; $\chi^{(2)}_{\rm EI} = \chi^{(3)} \cdot E_{\rm bi}$, $E_{\rm bi}$ is the built-in field in the surface layer of silicon. The detailed physical description of the electric-field-induced PE was discussed in our previous work[18].

Aside from KE and PE, PDE also exists in silicon because the applied electric field can change the carrier distribution. The change of the carrier density will induce the changes of the refractive index and the absorption factor according to the following equations[9]:

$$\begin{cases} \Delta n_{\rm PDE} = -6.2 \times 10^{-22} \Delta N - 6.0 \times 10^{-18} (\Delta P)^{0.8} \\ \Delta \alpha_{\rm PDE} = 6.0 \times 10^{18} \Delta N + 4.0 \times 10^{-18} \Delta P \\ (\text{for } \lambda = 1.3\,\mu\text{m}) \end{cases}, \quad (3)$$

where ΔN and ΔP are the changes of the densities of electrons and holes in silicon. From Eq. (3), we note that PDE cannot produce the birefringence because the change of the carrier density is not anisotropic, which is also the reason that PDE is insensitive to the polarization. Usually, ΔN and ΔP are proportional to the applied electric field $E = E_{\rm m}\cos(\Omega t)$; therefore, the frequency of the electro-optic signal induced by PDE is the same as that of the applied electric field.

Contrasting Eqs. (1)−(3), we know that the frequency response of KE is different from those of PE and PDE. PDE has no contribution to the birefringence; however, it influences the light intensity because of the change of the absorption factor. Thus, we can effectively distinguish these effects based on these differences.

In order to distinguish these electro-optic effects, we set up a transverse electro-optic measuring system (Fig. 1). A near-intrinsic (111)-Si crystal with the resistivity of approximately 4 000Ω cm and the carrier density of approximately 10^{12} cm^{-3} is used as the sample, the orientation and size of which are shown in Fig. 1(a). The configuration of the sample is a metal–insulator–semiconductor–insulator–metal (MISIM) planar capacitor. In order to prevent carriers from injecting into the silicon sample, two sufficiently thick (approximately 160 μm) polyester insulating layers are sandwiched between the metals and silicon. The measured total electric capacity of the sample structure without bias is approximately 16.5 pF. The dielectric constant of the insulating layers is approximately 3.0. The electric capacity of the insulating layers, C_i, is approximately 16.6 pF. The Debye length, $L_{\rm D}$, of the silicon sample is approximately 3.8 μm. The flat band capacity of the silicon sample is approximately 5.6 nF. Thus, only a small amount of applied voltage will drop on the space charge region of silicon. and most will drop on the insulating layers, and the small-signal modulating model will be satisfied.

The transverse electro-optic amplitude modulation structure is shown in Fig. 1(b). In our experiments, a 200-mW CW laser with the wavelength of 1.342 μm is used as the light source, and a 1-kHz sine signal from the signal generator is applied on the sample. The [111] axis (i.e., z axis) of the silicon sample and the polarizations of the polarizer are vertical in the space. The fast axes of the quarter-wave plate and the analyzer are, respectively, 45° and θ with respect to the [1$\bar{1}$0] axis (i.e., x axis). According to the Jones matrix calculation, the intensity of the output beam $I_{\rm out}$ from the analyzer can be obtained as

$$I_{\rm out} \approx I_{\rm in}\{1 - [\alpha_0 \pm \Delta\alpha(E)]l\}[1 - \Delta\phi(E)\sin 2\theta]/2, \quad (4)$$

where $I_{\rm in}$ is the intensity of input beam from the polarizer; l is the propagation length in silicon; $\alpha_0 \approx 3.5 \times 10^{-6}$ cm^{-1} is the absorption factor of silicon at the wavelength of 1.342 μm without the applied electric field[21], $\alpha_0 l << 1$ for our experiments. Here, $\Delta\alpha(E)$ is the change of the absorption factor caused by PDE defined in Eq. (3) and $\Delta\alpha(E)l << 1$ because the density of the free carrier is very low and the thick insulting layers prevent the carriers from injecting into the near-intrinsic silicon sample effectively. In addition, $\Delta\phi(E) << 1$, under the condition of small-signal modulation, is the phase difference between the ordinary light and the extraordinary light that describes the birefringence in silicon, including the KE component $\Delta\phi_{\rm KE}(E)$ and the PE component $\Delta\phi_{\rm PE}(E)$, which can be written as

$$\begin{aligned} \Delta\phi(E) &= \Delta\phi_{\rm KE}(E) + \Delta\phi_{\rm PE}(E) \\ &= 2\pi\Delta n_{\rm KE} l/\lambda + 2\pi\Delta n_{\rm PE} l/\lambda, \end{aligned} \quad (5)$$

where λ is the wavelength of probing beam in the free space. Therefore, the intensity of the output beam will be modulated by the applied electric field, and the modulated beam is received by the Ge photodetector. Finally,

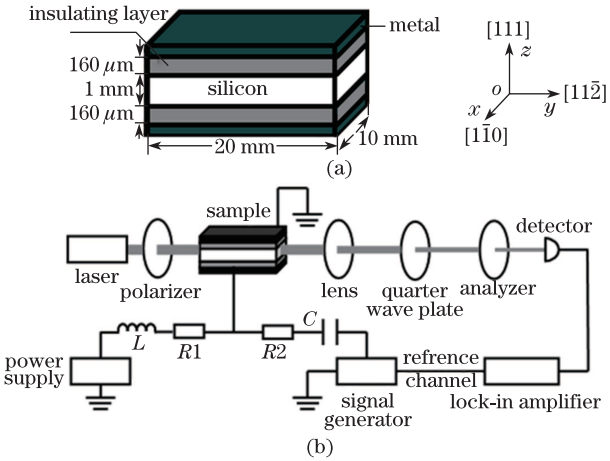

Fig. 1. Configuration of the silicon sample and the measuring system: (a) MISIM configuration of the silicon sample, the sizes and orientations of which are denoted; (b) experimental setup.

the photocurrent from the photodetector is connected into the lock-in amplifier, and the electro-optic signals are detected. Because the lock-in amplifier cannot detect the DC signal, the electro-optic signal detected by the lock-in amplifier could be written as follows based on Eqs. (4) and (5):

$$\begin{cases} V_{\rm eo} = V_1 + V_2 + V_3 + V_4 + V_5 \\ V_1 = CI_{\rm in}\Delta\alpha(E)l/2 \\ V_2 = CI_{\rm in}(1-\alpha_0 l)\pi l\Delta n_{\rm PE}\sin 2\theta/\lambda \\ V_3 = CI_{\rm in}(1-\alpha_0 l)\pi l\Delta n_{\rm KE}\sin 2\theta/\lambda \\ V_4 = CI_{\rm in}\Delta\alpha(E)\pi l\Delta n_{\rm PE}\sin 2\theta/\lambda \\ V_5 = CI_{\rm in}\Delta\alpha(E)\pi l\Delta n_{\rm KE}\sin 2\theta/\lambda \end{cases}, \quad (6)$$

where C is the constant relevant to the optical elements, the responsivity of the Ge photodetector, and the electrical system. Among these electro-optic signals, V_1 is only caused by PDE and independent of the azimuth θ of the analyzer, V_2 is only induced by PE, V_3 only results from KE, V_4 is caused by both PDE and PE, V_5 is induced by both PDE and KE, and V_2–V_5 are all dependent on the azimuth θ of the analyzer. Moreover, the frequencies of V_1 and V_2 should be identical with the modulating frequency Ω, the frequencies of V_3 and V_4 should be equal to 2Ω, and the frequency of V_5 should equal 3Ω.

We need to point out that KE induced by the modulating electric field $E(\Omega)$ is taken into account in this letter. Even though the optical electric field $E(\omega)$ and the DC built-in field $E_{\rm bi}(0)$ can also induce the index change based on the self-focusing effect and KE, respectively, these effects cannot be detected by the lock-in amplifier in the measuring system because they cannot cause the alternating change of the intensity of the probing beam. Moreover, through the interaction of the optical electric field $E(\omega)$ and the modulating electric field $E(\Omega)$, the third-order polarization, $P^3(\Omega) = 6\varepsilon_0\chi^{(3)}(\omega,-\omega,\Omega)\vdots E(\omega)E^*(\omega)E(\Omega)$ will be generated in the silicon sample, which could combine with the applied electric field $E(\Omega)$ and affect the polarization of the probing beam. However, the polarization field relative to $P^{(3)}(\Omega)$ should be much weaker than the applied electric field $E(\Omega)$; therefore, we can ignore the effect of $P^{(3)}(\Omega)$ on the receiver response.

We first measured the electro-optic signals with the frequency of Ω under different AC modulation voltages. The relationship between the electro-optic signals and the modulation voltage was obtained, shown in Fig. 2. Note that the electro-optic signals linearly increase with the modulation voltage. These electro-optic signals should include two kinds of components, V_1 and V_2, which are from PDE and PE respectively. As for the silicon sample with the MISIM structure, it can be taken as two back-to-back metal-insulator-semiconductor (MIS) capacitors. According to the theory of MIS capacitors, in strong inversion operation, the relation between the change of carrier density ΔN and the drive voltage $V_{\rm G}$ can be written as

$$\Delta N = \frac{\varepsilon_0\varepsilon_{\rm i}}{ed_{\rm i}t}(V_{\rm G} - V_{\rm TH}), \quad (7)$$

where ε_0 is the permittivity of free space, $\varepsilon_{\rm i}$ is the dielectric constant of the insulating layer, $d_{\rm i}$ is the thickness of the insulating layer, e is the elementary charge, t is the effective charge layer thickness, and $V_{\rm TH}$ is the threshold voltage. Therefore, according to Eqs. (3), (7), and (6), the electro-optic signal V_1 based on PDE is proportional to the modulation voltage. As for the electro-optic signal V_2, because $\alpha_0 l << 1$ and $\Delta\alpha(E)l << 1$, the magnitude V_2 is mainly decided by $\Delta n_{\rm PE}$. According to Eqs. (2) and (6), the electro-optic signal V_2 should also be proportional to the modulation voltage. Thus, the total electro-optic signal shown in Fig. 2 increases with the modulation voltage linearly.

In order to further distinguish between PE and PDE, we measured the dependence of electro-optic signals on the azimuth of the analyzer at the modulation voltages of 170, 100, and 50 V, respectively. The results are shown in Fig. 3. The larger the modulation voltage, the stronger the electro-optic signal. However, the modulation voltage does not affect the relationship between the electro-optic signal and the azimuth of the analyzer. In Fig. 3, the solid lines are theoretical fitted curves. The fitted functions are written as

$$\begin{cases} V_{\rm eo} = 0.35 + 4.2\sin 2(\theta+68) & (V_{\rm ac} = 50\ {\rm V}) \\ V_{\rm eo} = 2.5 + 8.6\sin 2(\theta+68) & (V_{\rm ac} = 100\ {\rm V}) \\ V_{\rm eo} = 3.3 + 14.2\sin 2(\theta+68) & (V_{\rm ac} = 170\ {\rm V}) \end{cases}. \quad (8)$$

From Eq. (8), the electro-optic signals include two components: first one is independent of the azimuth of analyzer, whereas the second is related to the azimuth θ. In

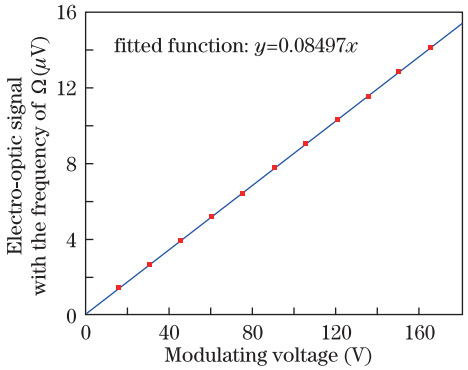

Fig. 2. Dependence of the electro-optic signal with the frequency of Ω on the AC modulating voltage for silicon sample with MISIM capacitor structure.

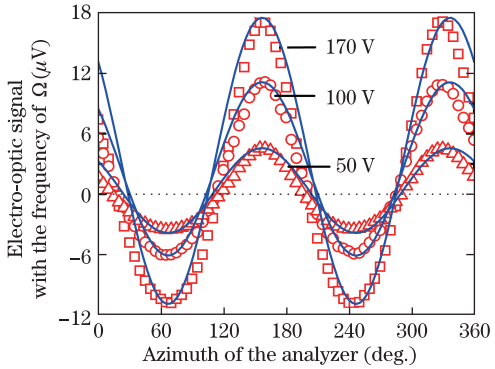

Fig. 3. Dependence of the electro-optic signal with the frequency of Ω on the azimuth θ of the analyzer under different modulating voltages.

fact, the component independent of the azimuth should be owed to PDE, which is the electro-optic signal V_1 defined by Eq. (6). The second component should be from PE, which is the electro-optic signal V_2 described by Eq. (6). Comparing these two components, PE is stronger than PDE in our near-intrinsic silicon samples.

The electro-optic signal with the frequency of 2Ω was also measured by setting the reference channel of the lock-in amplifier at the harmonic detection with the harmonic number of two. The results are shown in Fig. 4. Note that the electro-optic signal with the frequency of 2Ω is a quadratic function of the applied voltage. Actually, the measured electro-optic signals with the frequency of 2Ω should include, not only Kerr signal relevant to V_3 in Eq. (6), but also the quadratic electro-optic signal relevant to V_4 in Eq. (6). However, silicon is nearly transparent to photons with wavelengths larger than 1.1 μm; thus, the absorption factor α_0 of silicon is very small (approximately 3.5×10^{-6} cm^{-1} at the wavelength of 1.342 μm, that is $(1 - \alpha_0 l) >> \Delta\alpha(E)l$). Therefore compared with the Kerr signal, the electro-optic signal relevant to V_4 can be ignored in the experiments. Moreover, FKE can also be neglected in our experiments because FKE occurs only near the absorption edge of silicon and under the very strong electric-field. In our experiments, the wavelength of the probing beam is 1.342 μm, which is larger than the absorption edge 1.1 μm, and the electric field is not very strong (i.e., less than 10^3 V/cm). Actually, FKE can also be distinguished from other electro-optic effects in silicon because the index change Δn based on FKE is usually proportional to $E(\Omega)^m$ $(3 > m > 2)$. Here $E(\Omega)$ is the modulating electric field.

We also measured the dependence of the quadratic electro-optic signals with the frequency of 2Ω on the azimuth of the analyzer at the applied voltage of 170 V, as shown in Fig. 5. The solid line is the theoretical fitted curve. The fitted function is written as

$$V_{\rm eo} = -1.0 + 4.2\sin 2(\theta + 25). \quad (9)$$

From Eq. (9), we can see that the quadratic electro-optic signals also include two components: the constant independent of the azimuth θ of the analyzer and the component relevant to the azimuth θ. Based on Eq. (6), the latter is the Kerr signal induced by the modulating field $E(\Omega)$, whereas the former may include background noise and thermo-optic signal likely resulting from the feeble electric current (several microamperes) and the laser irradiation in the silicon sample.

According to the Eq. (6), the total electro-optic signals should also include the component V_5 with the frequency of 3Ω, which is determined by the product of $\Delta\alpha(E)$ and $\Delta n_{\rm KE}$. Compared with V_1–V_4, V_5 is much smaller. We measured it by setting the reference channel of the lock-in amplifier at the harmonic detection with the harmonic number of three. However, this signal is so small that it cannot be detected.

In conclusion, a method for distinguishing the electro-optic effects such as KE, PE, and PDE in silicon crystals

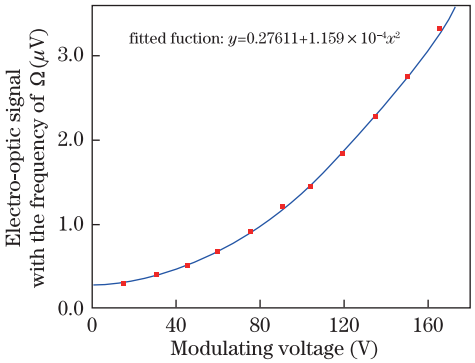

Fig. 4. Quadratic electro-optic signal with the frequency of 2Ω versus AC modulating voltage.

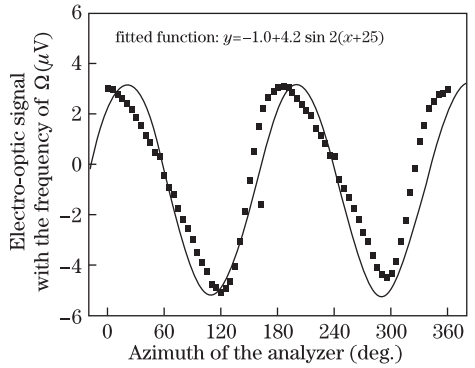

Fig. 5. Dependence of the quadratic electro-optic signal with the frequency of 2Ω on the azimuth θ of the analyzer.

is put forward. This method is mainly based upon the fact that these electro-optic effects have different frequency characteristics and polarization dependencies. Using our method, we experimentally measure and distinguish these electro-optic effects in the (111)-cut near-intrinsic silicon crystal. The results indicate that PE resulting from the surface electric field and surface strain is the major electro-optic effect in the near-intrinsic silicon sample. According to our experimental results, the signal of PE is over four times larger than that of KE or PDE. Because these effects are considerable, they must be considered in designing the silicon-based opto-electronic devices. They may also be used as tools to study the properties of surfaces and interfaces of silicon devices. The method for distinguishing these effects might play an important role in designing and fabricating the silicon-based photonic devices. The method is also suitable for investigating the electro-optic effects in other isotropic materials with inversion symmetry (e.g., electro-optic effects in diamonds[22]).

This work was partially supported by the National High-technology Research and Development Program of China (No. 2009AA03Z419), the National Natural Science Foundation of China (Nos. 60976037 and 61077026), the Joint Research Projects of NSFC-RFBR (Nos. 60811120023 and 61111120097), and the Natural Science Foundation of Jilin Province, China (No. 201215019).

References

1. R. A. Soref, Proc. IEEE **81,** 1687 (1993).
2. M. Salib, L. Liao, R. Jones, M. Morse, A. Liu, D. Samara-Rubio, D. Alduino, and M. Paniccia, Intel Technol. J. **8,** 143 (2004).
3. B. Jalali and S. Fathpour, J. Lightwave Technol. **24,** 4600 (2006).
4. A. Liu, R. Jones, L. Liao, D. Samara-Rubio, D. Rubin, O. Cohen, R. Nicolaescu, and M. Paniccia, Nature **427,** 615 (2004).
5. Q. Xu, B. Schmidt, S. Pradhan, and M. Lipson, Nature **435,** 325 (2005).
6. M. Zhu, Z. Zhou, and D. Gao, Chin. Opt. Lett. **7,** 924 (2009).
7. R. L. Espinola, M-C. Tsai, J. T. Yardley, and R. M. Osgood, IEEE Photon. Technol. Lett. **15,** 1366 (2003).
8. G. Cocorullo, M. Iodice, I. Rendina, and P. M. Sarro, IEEE Photon. Technol. Lett. **7,** 363 (1995).
9. R. A. Soref and B. R. Bennett, IEEE J. Quantum Electron. **23,** 123 (1987).
10. H. K. Tsang and Y. Liu, Semicond. Sci. Technol. **23,** 064007 (2008).
11. Z. Chen, J. Zhao, Y. Zhang, G. Jia, X. Liu, C. Ren, W. Wu, J. Sun, K. Cao, S. Wang, and B. Shi, Appl. Phys. Lett. **92,** 251111 (2008).
12. A. Frova, P. Handler, F. A. Germano, and D. E. Aspnes, Phys. Rev. **145,** 575 (1966).
13. G. V. Treyz, P. G. May, and J.-M. Halbout, Appl. Phys. Lett. **59,** 771 (1991).
14. O. A. Aktsipetrov, A. A. Fedyanin, A. V. Melnikov, E. D. Mishina, and A. N. Rubtsov, Phys. Rev. B **60,** 8924 (1999).
15. P. Godefroy, W. de Jong, C. W. van Hasselt, M. A. C. Devillers, and Th. Rasing, Appl. Phys. Lett. **68,** 1981 (1996).
16. N. K. Hon, K. K. Tsia, D. R. Solli, and B. Jalali, Appl. Phys. Lett. **94,** 091116 (2009).
17. J. Zhao, Q. Chen, Z. Chen, G. Jia, W. Su, Y. Jiang, Z. Yan, T. V. Dolgova, O. A. Aktsipetrov, and H. Sun, Opt. Lett. **34,** 3340 (2009).
18. J. Zhu, Z. Chen, X. Liu, Y. Gao, J. Mu, Z. Wang, W. Han, and G. Jia, Opt. Laser Technol. **44,** 582 (2012).
19. R. S. Jacobsen, K. N. Andersen, P. I. Borel, J. Fage-Pedersen, L. H. Frandsen, O. Hansen, M. Kristensen, A. V. Lavrinenko, G. Moulin, H. Ou, C. Peucheret, B. Zsigri, and A. Bjarklev, Nature **441,** 199 (2006).
20. B. Chmielak, M. Waldow, C. Matheisen, C. Ripperda, J. Bolten, T. Wahlbrink, M. Nagel, F. Merget, and H. Kurz, Opt. Express **19,** 17212 (2011).
21. M. A. Green and M. J. Keevers, Prog. Photovolt. **3,** 189 (1995).
22. J. Zhao, G. Jia, X. Liu, Z. Chen, J. Tang, and S. Wang, Chin. Opt. Lett. **8,** 685 (2010).